Anisotropic distributions in a multiphase transport model

You Zhou,[1,*] Kai Xiao,[2,3] Zhao Feng,[2] Feng Liu,[2,†] and Raimond Snellings[4]
[1]*Niels Bohr Institute, University of Copenhagen, Blegdamsvej 17, 2100 Copenhagen, Denmark*
[2]*Key Laboratory of Quark and Lepton Physics (MOE) and Institute of Particle Physics, Central China Normal University, Wuhan 430079, China*
[3]*South-Central University for Nationalities, Wuhan 430074, China*
[4]*Utrecht University, P.O. Box 80000, 3508 TA Utrecht, The Netherlands*
(Received 14 August 2015; published 17 March 2016)

With a multiphase transport (AMPT) model we investigate the relation between the magnitude, fluctuations, and correlations of the initial state spatial anisotropy ε_n and the final state anisotropic flow coefficients v_n in Au+Au collisions at $\sqrt{s_{\rm NN}} = 200$ GeV. It is found that the relative eccentricity fluctuations in AMPT account for the observed elliptic flow fluctuations, both are in agreement with the elliptic flow fluctuation measurements from the STAR collaboration. In addition, the studies based on two- and multiparticle correlations and event-by-event distributions of the anisotropies suggest that the elliptic-power function is a promising candidate of the underlying probability density function of the event-by-event distributions of ε_n as well as v_n. Furthermore, the correlations between different order symmetry planes and harmonics in the initial coordinate space and final state momentum space are presented. Nonzero values of these correlations have been observed. The comparison between our calculations and data will, in the future, shed new insight into the nature of the fluctuations of the quark-gluon plasma produced in heavy ion collisions.

DOI: 10.1103/PhysRevC.93.034909

I. INTRODUCTION

One of the fundamental questions in the phenomenology of quantum chromodynamics (QCD) is what the properties of matter are at the extreme densities and temperatures where quarks and gluons are in a new state of matter, the so-called quark gluon plasma (QGP). Collisions of high-energy heavy ions, at the Brookhaven Relativistic Heavy Ion Collider (RHIC) and the CERN Large Hadron Collider (LHC), allow us to create and study the properties of such a system in the laboratory.

The azimuthal anisotropy in particle production is, at these energies, an observable which provides experimental information on the equation of state and the transport properties of the QGP. This anisotropy is usually characterized by the Fourier flow coefficients [1],

$$v_n = \langle \cos[n(\varphi - \Psi_n)\rangle, \quad \text{or equivalently}$$
$$v_n = \langle e^{in\varphi} e^{-in\Psi_n}\rangle, \tag{1}$$

where φ is the azimuthal angle of the particles, Ψ_n is the $n^{\rm th}$-order flow plane (or named final state symmetry plane) angle, and $\langle\rangle$ denotes an average over the selected particles and events.

In the last decade, the elliptic flow v_2 [2–8], which is considered to correspond to the elliptical shape of the spatial overlap region in the system created in the collisions [9], has received a lot of experimental and theoretical attention. For a recent summary see [10–15]. More recently, higher odd and even anisotropic flow coefficients are found to be also very important [16]. Hydrodynamic calculations predict that these higher harmonics, such as the triangular flow v_3, are more sensitive to the shear viscosity to entropy density ratio η/s of the QGP than v_2 [17]. Furthermore, it is realized that the correlations between the symmetry planes and flow harmonics are sensitive to both the initial state and η/s [18–20]. The combined analysis of both ε_n and v_n distributions for a single harmonic, and the correlations between different orders of symmetry planes (direction of the flow vector) and flow harmonics (magnitude of the flow vector) could yield powerful constraints on both initial conditions and properties of the QGP. However, so far the investigation of the above mentioned combined analysis using a transport model was still lacking.

In this paper, we present the calculations of initial state anisotropies and final state anisotropic flow in Au+Au collisions at $\sqrt{s_{\rm NN}} = 200$ GeV using the AMPT model [21]. We also investigate the relation between the magnitude, fluctuations, and correlations of the initial state spatial eccentricity and final state anisotropic flow coefficients. In addition, the correlations between different order symmetry planes and harmonics will be investigated in both the initial and final state, which will help us understand how they are modified during the expansion of the system.

II. A MULTIPHASE TRANSPORT MODEL

A multiphase transport (AMPT) model [21] with a so-called string melting scenario was used for these studies. The model consists of four main stages: initial conditions, partonic interactions, hadronization, and finally hadronic rescattering.

The initial conditions, which include the spatial and momentum distributions of minijet partons and soft string excitations, are obtained from the HIJING model [22]. The strings are converted into partons and the next stage, which models the interactions between all the partons, is based on ZPC

*you.zhou@cern.ch
†fliu@mail.ccnu.edu.cn

[23]. The partonic cascade model ZPC presently includes only two-body processes with cross sections obtained from pQCD with screening masses. In ZPC, the default value of the cross section is 3 mb. The transition from partonic to hadronic matter is modeled by a simple coalescence model, which combines two quarks into mesons and three quarks into baryons [24]. Finally, to describe the dynamics of the subsequent hadronic stage, a hadronic cascade based on the ART model [25] is used. In this analysis, we used the default input parameters of AMPT with string melting suggested in Ref. [21]. The results are presented as a function of centrality, which was determined by impact parameter **b**, as used in Refs. [26,27]. The possible effects of the fluctuations of impact parameters will be discussed in next section.

III. ANALYSIS METHOD AND DEFINITIONS

In this paper the anisotropic flow is calculated using the two- and multiparticle cumulants method [28,29], which was widely used at RHIC [30] and at the LHC [6,31]. In this method, both two- and multiparticle azimuthal correlations are analytically expressed in terms of a Q vector, which is defined as

$$Q_n = \sum_{i=1}^{M} e^{in\varphi_i}, \tag{2}$$

where M is the multiplicity of the selected particles and φ is their azimuthal angle.

The single-event average two-particle azimuthal correlations can be calculated via

$$\langle 2\rangle = \frac{|Q_n|^2 - M}{M(M-1)}. \tag{3}$$

From this the event averaged two-particle correlations, and the two-particle cumulants can be obtained using

$$c_n\{2\} \equiv \langle\langle 2\rangle\rangle = \frac{\sum_{\text{events}}(W_{\langle 2\rangle})_i \langle 2\rangle_i}{\sum_{\text{events}}(W_{\langle 2\rangle})_i}, \tag{4}$$

where $W_{\langle 2\rangle}$ is the event weight. To minimize the effect of the varying multiplicity in certain centrality class determined by **b**, we use the number of particle pairs as the event weight proposed in Ref. [32]

$$W_{\langle 2\rangle} \equiv M(M-1). \tag{5}$$

The anisotropic flow from two-particle cumulants, denoted as $v_n\{2\}$, is finally obtained from

$$v_n\{2\} = \sqrt{c_n\{2\}}. \tag{6}$$

Unfortunately, the $v_n\{2\}$ contains contributions from so-called nonflow effects, which are additional azimuthal correlations not associated with the common symmetry planes, e.g., resonance decays, jet fragmentation, and Bose-Einstein correlations. They can be suppressed by appropriate kinematic cuts and therefore one can introduce a gap in pseudorapidity between the particles used in the two-particle Q-cumulant method [33]. For this we divide the whole event into two subevents, A and B, which are separated by a pseudorapidity gap $|\Delta\eta|$. This modifies Eq. (3) to

$$\langle 2\rangle_{\Delta\eta} = \frac{Q_n^A \cdot Q_n^{B*}}{M_A \cdot M_B}, \tag{7}$$

where Q_n^A and Q_n^B are the flow vectors from subevents A and B, with M_A and M_B the corresponding multiplicities. The event weight from Eq. (5) in this case becomes

$$W_{\langle 2\rangle_{\Delta\eta}} \equiv M_A \cdot M_B. \tag{8}$$

Finally, inserting Eqs. (7) and (8) into Eq. (4), the v_n from a two-particle cumulant with a $\Delta\eta$ gap is given by

$$v_n\{2,|\Delta\eta|\} = \sqrt{\langle\langle 2\rangle\rangle_{\Delta\eta}}. \tag{9}$$

Instead of using kinematic cuts, the collective nature of anisotropic flow itself can be exploited to suppress nonflow contributions. Using multiparticle instead of two-particle cumulants the aforementioned nonflow effects are strongly suppressed and no additional kinematic cuts are required. The v_n calculated using cumulants are denoted as $v_n\{k\}$, where k is 2,4,6...,m for the m-particle cumulant. Following the Q-cumulant method [29], the single event average four- and six-particle correlations can be calculated as

$$\begin{aligned}
\langle 4\rangle =& [\,|Q_n|^4 + |Q_{2n}|^2 - 2\cdot\mathrm{Re}(Q_{2n}Q_n^*Q_n^*) \\
&- 2[2(M-2)\cdot|Q_n|^2 - M(M-3)]\,]/ \\
&[M(M-1)(M-2)(M-3)], \\
\langle 6\rangle =& [\,|Q_n|^6 + 9|Q_{2n}|^2|Q_n|^2 - 6\cdot\mathrm{Re}(Q_{2n}Q_nQ_n^*Q_n^*Q_n^*) \\
&+ 4\cdot\mathrm{Re}(Q_{3n}Q_n^*Q_n^*Q_n^*) - 12\cdot\mathrm{Re}(Q_{3n}Q_{2n}^*Q_n^*) \\
&+ 18(M-4)\cdot\mathrm{Re}(Q_{2n}Q_n^*Q_n^*) + 4|Q_{3n}|^2 \\
&- 9(M-4)\big(|Q_n^4| + |Q_{2n}|^2\big) + 18(M-2)(M-5)|Q_n|^2 \\
&- 6M(M-4)(M-5)\,]/ \\
&[M(M-1)(M-2)(M-3)(M-4)(M-5)].
\end{aligned} \tag{10}$$

Then the multiparticle cumulants are obtained from

$$\begin{aligned}
c_n\{4\} &= \langle\langle 4\rangle\rangle - 2\,\langle\langle 2\rangle\rangle^2, \\
c_n\{6\} &= \langle\langle 6\rangle\rangle - 9\,\langle\langle 2\rangle\rangle\cdot\langle\langle 4\rangle\rangle + 12\,\langle\langle 2\rangle\rangle^3,
\end{aligned} \tag{11}$$

where $\langle\langle\rangle\rangle$ denotes the average over all particles over all events. In the end the v_n from four- and six-particle cumulants, denoted as $v_n\{4\}$ and $v_n\{6\}$, are obtained using

$$v_n\{4\} = \sqrt[4]{-c_n\{4\}}, \quad v_n\{6\} = \sqrt[6]{c_n\{6\}}. \tag{12}$$

The two- and multiparticle cumulants have different contributions from flow fluctuations. The contribution from flow fluctuations is positive for the two-particle cumulant and negative for the multiparticle cumulant [34,35]. When nonflow effects are negligible for the two-particle cumulant, and if $\sigma_{v_n} \ll \overline{v}_n$, the v_n from the cumulants are up to order $\sigma_{v_n}^2$ given by

$$\begin{aligned}
v_n\{2\}^2 &\approx \overline{v}_n^2 + \sigma_{v_n}^2, \\
v_n\{4\}^2 &\approx \overline{v}_n^2 - \sigma_{v_n}^2, \\
v_n\{6\}^2 &\approx \overline{v}_n^2 - \sigma_{v_n}^2,
\end{aligned} \tag{13}$$

where $\overline{v}_n$ and σ_{v_n} are the mean and standard deviation of the v_n distributions, respectively. In the special case that the underlying probability density function ($p.d.f.$) of v_n is described by a Bessel-Gaussian function, Eq. (13) is an exact solution, independent of the magnitude of the flow fluctuations. This shows that for a Bessel-Gaussian $p.d.f.$ all the multiparticle cumulants will be identical.

It is thought that the development of anisotropic flow is controlled by the anisotropies in the pressure gradients which in turn depend on the shape and structure of the initial density profile. The latter can be characterized, in analogy with the flow Fourier coefficients and flow angles of Eq. (1), by a set of harmonic anisotropy coefficients ε_n and associated symmetry angles Φ_n of the initial spatial distribution:

$$\varepsilon_n e^{in\Phi_n} \equiv -\frac{\int r\,dr\,d\phi\, r^n e^{in\phi}\, e(r,\phi)}{\int r\,dr\,d\phi\, r^n e(r,\phi)}\ (n > 1), \tag{14}$$

where $e(r,\phi)$ is the initial energy density distribution in the plane transverse to the beam direction. Also these anisotropy coefficients can be calculated using cumulants and the same relation between $\overline{\varepsilon}_n$ and σ_{ε_n} follows as in Eq. (13), replacing v_n with ε_n.

IV. RESULTS AND DISCUSSION

The centrality dependence of v_2 from the AMPT model calculations is shown in Fig. 1(a). For the two-particle cumulant calculations, we plot both $v_2\{2\}$ from Eq. (6) and $v_2\{2,|\Delta\eta| > 1\}$ from Eq. (9). It is seen that the $v_2\{2,|\Delta\eta| > 1\}$ is compatible with $v_2\{2\}$, which indicates that short-range nonflow contributions are very small in AMPT. Figure 1(a) also shows the calculated $v_2\{4\}$ and $v_2\{6\}$. Because the nonflow contributions to the integrated flow are very small, the observed significant difference between $v_2\{2\}$ and $v_2\{4\}$ is from elliptic flow fluctuations. In addition we observe that there is very good agreement between $v_2\{4\}$ and $v_2\{6\}$. This seems to agree with the expectation that the underlying $p.d.f.$ is a Bessel-Gaussian function, which predicts $v_2\{4\} = v_2\{6\}$. However, it is still important to point out that in fact $v_2\{4\} \approx v_2\{6\}$ is valid irrespectively of the details of the underlying model of flow fluctuations, under the assumption $\sigma_{v_n} \ll \overline{v_n}$ [32].

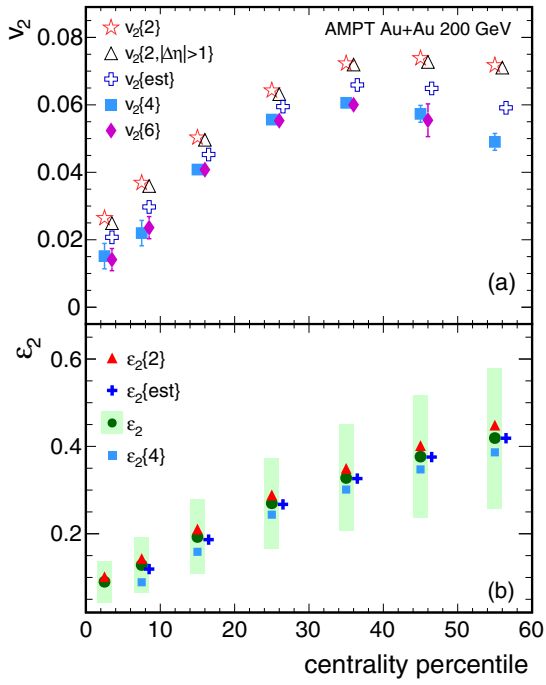

FIG. 1. Centrality dependence of (a) v_2 and (b) ε_2 in Au+Au collisions at $\sqrt{s_{\rm NN}} = 200$ GeV in AMPT. For the definition of the symbols see text.

From $v_2\{2,|\Delta\eta| > 1\}$ and $v_2\{4\}$, we can estimate $\overline{v}_2$ in Eq. (13) using

$$\overline{v}_2\{\text{est}\} = \sqrt{\frac{v_2\{2,|\Delta\eta| > 1\}^2 + v_2\{4\}^2}{2}}. \tag{15}$$

Figure 1(b) shows ε_2 as a function of centrality. Here ε_2 can be calculated from the initial spatial parton distributions in the AMPT model. The relative fluctuation of ε_2, named σ_{ε_2}, is shown by the green band as the uncertainty of $\overline{\varepsilon}_2$. The $\varepsilon_2\{2\}$ and $\varepsilon_2\{4\}$ correspond to the two- and four-particle cumulant definitions but are evaluated using the initial spatial coordinates. We see that $\varepsilon_2\{2\}$, ε_2, and $\varepsilon_2\{4\}$ increase monotonically up to 60% centrality percentile. In contrast, the v_2, plotted in Fig. 1(a), starts to saturate or decrease from 40% centrality percentile. This difference between the centrality dependence of v_2 and ε_2 is generally understood to be because of the fact that the efficiency of converting the initial eccentricity into final elliptic flow decreases towards peripheral collisions because of the decreasing number of reinteractions in a smaller system.

From the calculated anisotropic flow, we can investigate the relation between the fluctuations in ε_n and v_n. In Fig. 2(a) we plot the centrality dependence of the elliptic flow fluctuations σ_{v_2} estimated via

$$\sigma_{v_2} = \sqrt{\frac{v_2\{2,|\Delta\eta| > 1\}^2 - v_2\{4\}^2}{2}}. \tag{16}$$

We find that σ_{v_2} increases toward peripheral collisions and its magnitude is significant compared to the magnitude of v_2. Assuming $v_2 \propto \varepsilon_2$ and using Eq. (13), we also have $v_2\{2\} \propto \varepsilon_2\{2\}$ and $\sigma_{v_2} \propto \sigma_{\varepsilon_2}$. Hence, Fig. 2(a) also shows the scaled σ_{ε_2} calculated as $\sigma_{\varepsilon_2} = \sqrt{(\varepsilon_2\{2\}^2 - \varepsilon_2\{4\}^2)/2}$. It shows that the eccentricity fluctuations describe the centrality dependence of the elliptic flow fluctuations quite well, which might indicate that they are the dominant contribution for the observed elliptic flow fluctuations.

The estimated relative flow fluctuations, can be calculated using

$$R_{v_{2,4}} = \sqrt{\frac{v_2\{2,|\Delta\eta| > 1\}^2 - v_2\{4\}^2}{v_2\{2,|\Delta\eta| > 1\}^2 + v_2\{4\}^2}} \approx \frac{\sigma_{v_2}}{\overline{v}_2}, \tag{17}$$

and its centrality dependence is shown in Fig. 2(b). The magnitude of the relative fluctuations ranges from 0.4 to 0.6 in central to mid-peripheral collisions. This shows that the assumption $\sigma_{v_2} \ll \overline{v}_2$ does not hold for these centralities.

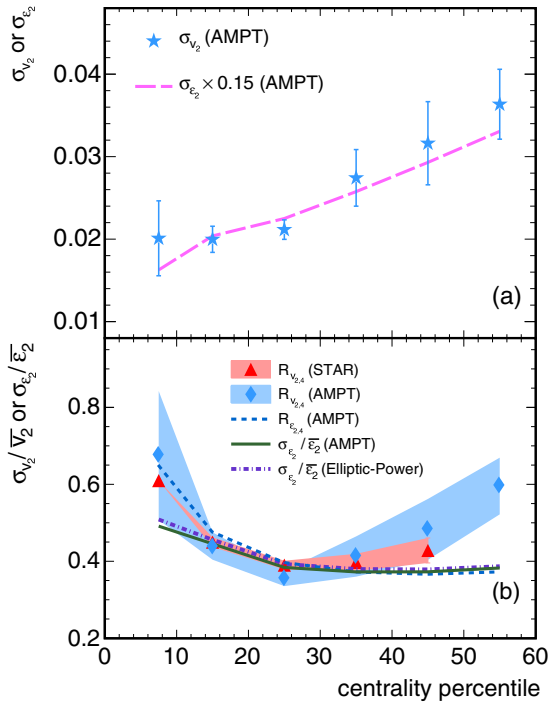

FIG. 2. Centrality dependence of (a) elliptic flow fluctuation and (b) relative elliptic flow (eccentricity) fluctuations in Au+Au collisions at 200 GeV in AMPT StringMelting. (a) The full stars are the estimated elliptic flow fluctuation σ_{v_2} and the dashed line is the relative eccentricity fluctuations scaled by a factor of 0.15; (b) the estimated relative elliptic flow fluctuation $R_{v_{2,4}}$, and the relative eccentricity and true eccentricity fluctuation for the AMPT model are shown using full diamonds, a dashed line, and solid line. In addition, the measurement from the STAR Collaboration are plotted using full triangles and the shadow shows its uncertainty [30].

The estimated relative eccentricity fluctuations $R_{\varepsilon_{2,4}}$ can be calculated analogously to the $R_{v_{2,4}}$:

$$R_{\varepsilon_{2,4}} = \sqrt{\frac{\varepsilon_2\{2\}^2 - \varepsilon_2\{4\}^2}{\varepsilon_2\{2\}^2 + \varepsilon_2\{4\}^2}} \approx \frac{\sigma_{\varepsilon 2}}{\bar{\varepsilon}_2}, \tag{18}$$

and compared to $R_{v_{2,4}}$. This comparison does not depend on the assumption that the relative fluctuations are small or the underlying $p.d.f.$ is a Bessel Gaussian. We notice that the $R_{\varepsilon_{2,4}}$ [also plotted in Fig. 2(b)] is compatible with $R_{v_{2,4}}$ for central and mid-central collisions. To test if this is only accidental we also study the v_2 in AMPT with an approximately three times larger partonic cross section (10 mb). The magnitudes of both $v_2\{2\}$ and $v_2\{4\}$ increase significantly, however, the consistency between $R_{\varepsilon_{2,4}}$ and $R_{v_{2,4}}$ continues to hold. This is expected if the relative elliptic flow fluctuations depend only on the eccentricity fluctuations, which again shows that eccentricity fluctuations play an important role in the development of elliptic flow fluctuations in the AMPT model.

In addition, we calculate directly from the initial state of the AMPT model the true relative eccentricity fluctuations $\sigma_{\varepsilon_2}/\bar{\varepsilon}_2$ [plotted as the the green solid line in Fig. 2(b)]. The results are consistent with the estimated relative eccentricity fluctuations in the 20%–50% centrality percentile, while they deviate for central and peripheral collisions. Because the assumption $\sigma_{\varepsilon_2} \ll \varepsilon_2$ is not satisfied over the whole centrality range this indicates that for 20%–50% the fluctuations might be approximately described by a Bessel Gaussian but to describe the overall event-by-event v_2 distributions, we need to search for a better candidate of the underlying $p.d.f.$ To see how these fluctuations compare to experimental data we compare to STAR measurements [30]. The relative elliptic flow fluctuations measured in Au+Au collisions at 200 GeV are plotted in Fig. 2(b) and are in very good agreement with the AMPT model calculations.

Hydrodynamic calculations have shown that in a given event, the v_n is a linear response to the initial anisotropy ($v_n = k_n\,\varepsilon_n$), for $n = 2, 3$ [36]. In the discussion above, we found that the elliptic flow and its fluctuations can be nicely described by the initial eccentricity together with its fluctuations. To further constrain the underlying $p.d.f.$ of the v_n and ε_n distributions, we study the event-by-event distributions of ε_n, simulated by AMPT.

In this study, the event-by-event ε_n distributions are investigated in the selected centrality classes. To better extract the information on the underlying $p.d.f.$ of the ε_n distributions, several candidate functions are used in this paper. One popular parametrization of the ε_n distribution is the Bessel-Gaussian distributions [37]:

$$p(\varepsilon_n) = \frac{\varepsilon_n}{\sigma^2} I_0\left(\frac{\varepsilon_n \varepsilon_n}{\sigma^2}\right) \exp\left(-\frac{\varepsilon_0^2 + \varepsilon_n^2}{2\sigma^2}\right), \tag{19}$$

where ε_0 is the anisotropy with respect to the reaction plane and σ is the fluctuation in the spatial anisotropy. It was already shown in this paper as well as in previous studies [37,38] that a Bessel-Gaussian distribution nicely describes the ε_2 distributions for mid-central collisions. However, it is not expected to work perfectly in peripheral collisions because of the lack of a constraint that $\varepsilon_2 < 1$ in each event [39]. To fix this problem, a simple one-parameter power-law distribution [40],

$$p(\varepsilon_n) = 2\alpha\,\varepsilon_n \left(1 - \varepsilon_n^2\right)^{\alpha - 1}, \tag{20}$$

was proposed to parametrize the fluctuation-driven anisotropies. Here α quantifies the fluctuations.

Recently, a new function, named the "elliptic power" distribution was proposed in Ref. [39] as

$$p(\varepsilon_n) = \frac{\alpha\,\varepsilon_n}{\pi}\left(1 - \varepsilon_0^2\right)^{\alpha + \frac{1}{2}} \int_0^{2\pi} \frac{\left(1 - \varepsilon_n^2\right)^{\alpha - 1} d\phi}{(1 - \varepsilon_0\,\varepsilon_n \cos\phi)^{2\alpha + 1}}, \tag{21}$$

where α and ε_0 have the same meaning as above. In our paper, these three candidates of the underlying $p.d.f.$s are fitted to the ε_n distributions in the AMPT model.

Figure 3 shows the ε_2 distributions in the centrality range 0%–5%, 30%–40%, and 60%–70% from the AMPT initial state. We fit the three distributions with the elliptic-power (solid lines), power-law (dash line), and Bessel-Gaussian functions (dot-dash line). It is shown that in 0%–5% these three functions give consistent results and they all fit the ε_2 distributions quite well. It is understood that in the case where $\varepsilon_0 \ll 1$ (small anisotropy from the reaction plane) and where $\alpha > 1$ (strong fluctuations), the elliptic power distribution turns into a Bessel-Gaussian distribution; while with $\varepsilon_0 = 0$

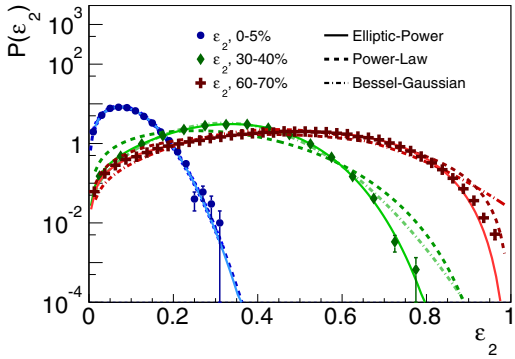

FIG. 3. ε_2 distributions in the AMPT initial state.

(anisotropy is solely from fluctuations), the elliptic power distribution reduces to a power-law distribution. The nice agreement between the three functions shows that the ε_0 must be very small, which means that the eccentricity is generated mainly by fluctuations. In 30%–40%, it is clear that only the elliptic-power function agrees with the ε_2 distributions. For more peripheral collisions, the elliptic-power function describes the ε_2 distributions still quite well, while the Bessel Gaussian can't quantitatively reproduce the ε_2 distributions. The power-law function, on the other hand, is not expected to describe the ε_2 distributions in noncentral collisions, because the eccentricity from the reaction plane (ε_0) is missing and for noncentral collisions ε_0 is nonzero and important to describe the ε_2 distributions. Furthermore, we calculate $\sigma_{\varepsilon_2}/\overline{\varepsilon}_2$ from the elliptic-power function with parameters extracted from the fits of the ε_2 distributions. The result shown in Fig. 2(b) is in nice agreement with the $\sigma_{\varepsilon_2}/\overline{\varepsilon}_2$ directly from the AMPT initial state. For describing all the centralities the elliptic-power function gives the best description of the ε_2 distributions. Unfortunately, the expectation of a 1% difference between the four- and six-particle cumulants [39] from the elliptic-power function cannot be tested with the current statistics.

It is shown in hydrodynamic calculations that the higher harmonic flow coefficients are more sensitive to both the kinematic viscosity and to the initial geometry and its fluctuations [17]. In the absence of fluctuations v_3 is zero because of symmetry constraints. Figure 4(a) shows the centrality dependence of v_3 obtained for AMPT events from different analysis methods. If v_3 is from event-by-event fluctuations in the initial spatial density distributions we would expect that there is no, or only a very small, correlation between both the reaction plane angle $\Psi_{\rm RP}$ (spanned by the impact parameter vector and the beam direction) and the angle of the second-order flow plane Ψ_2 with respect to the third-order flow plane Ψ_3. The correlations between Ψ_3 and $\Psi_{\rm RP}$ can be studied via

$$\begin{aligned} v_3\{\Psi_{\rm RP}\} &= \langle\langle \cos 3(\varphi - \Psi_{\rm RP})\rangle\rangle \\ &= \langle\langle \cos 3(\varphi - \Psi_3)\cos 3(\Psi_3 - \Psi_{\rm RP})\rangle\rangle \\ &= \langle v_3 \langle \cos 3(\Psi_3 - \Psi_{\rm RP})\rangle\rangle. \end{aligned} \quad (22)$$

In Fig. 4(a) we observe that $v_3\{\Psi_{\rm RP}\}$ is consistent with zero. It indeed shows that there is no correlation (or an extremely weak correlation) between Ψ_3 and $\Psi_{\rm RP}$ in the presented centrality range. We also see that both the $v_3\{2\}$ and $v_3\{4\}$ are

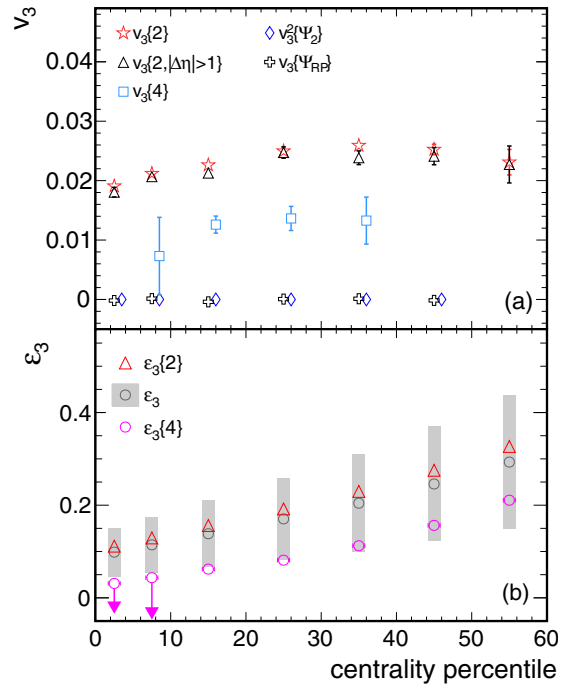

FIG. 4. (a) Centrality dependence of v_3 in Au+Au collisions at 200 GeV from AMPT model calculations. The open stars (red), triangles (black), circles (gray), diamonds (blue), and crosses (black) for $v_3\{2\}$, $v_3\{2,|\Delta\eta| > 1\}$, $v_3^2\{\Psi_2\}$, and $v_3\{\Psi_{\rm RP}\}$, respectively. (b) The corresponding ε_3 as a function of centrality.

nonzero and show only a weak centrality dependence, which is in qualitative agreement with earlier observations based on hydrodynamic model calculations [17].

In Fig. 4(b) the corresponding $\varepsilon_3\{2\}$, $\varepsilon_3\{4\}$, and ε_3 are plotted which, in contrast with $v_3\{2\}$ and $v_3\{4\}$, increase with increasing centrality by a factor two; this difference might be from strong viscous damping effects on v_3 compared to v_2 [17]. The expectation that $\varepsilon_3\{4\} = \varepsilon_3\{\Psi_{\rm RP}\} = 0$ if the $p.d.f.$ were a Bessel-Gaussian function is not observed in the 5%–40 % centrality percentile range, as is shown in Fig. 4.[1] Similar nonzero $\varepsilon_3\{4\}$ were found for wider centrality ranges from both MC-Glauber and MC-KLN calculations [41]. In fact, nonzero values of not only $v_3\{4\}$ but also $v_3\{6\}$ have been measured in experiments [42]. Compared to the Bessel-Gaussian distribution, which was the widely used description of the underlying $p.d.f.$, it shows in Fig. 5 that the elliptic-power function seems to give an improved description of $\sigma_{\varepsilon_3}/\varepsilon_3$ and agrees with a nonzero value of the multiparticle cumulants of ε_3 and v_3.

For completeness, Fig. 6 shows the ε_3 distributions in the centrality range 0%–5%, 30%–40%, and 60%–70% from the AMPT initial state. Similar to the study of the ε_2 distributions, we fit all the ε_3 distributions with the elliptic-power (solid lines), power-law (dash line), and Bessel-Gaussian functions

[1]Because of large statistical fluctuations in most central collisions, $\varepsilon_3^2\{4\} < 0$, we therefore presented $\sqrt{-\varepsilon_3^2\{4\}}$ in most central collisions and the arrows show the range from $-\sqrt{-\varepsilon_3^2\{4\}}$ to $\sqrt{-\varepsilon_3^2\{4\}}$.

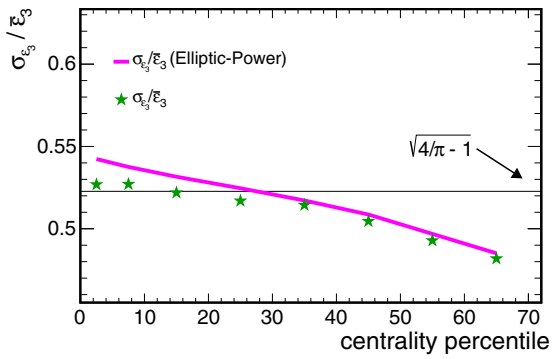

FIG. 5. $\sigma_{\varepsilon_3}/\bar{\varepsilon}_3$ distributions in AMPT.

(dot-dash line). It is seen that the Bessel-Gaussian function reproduces the ε_3 fairly well except for peripheral collisions. Nevertheless, the expectation of a Bessel Gaussian, which is $\varepsilon_3\{4\} = \varepsilon_3\{6\} = \varepsilon_3\{\mathrm{RP}\} = 0$ (as well as $v_3\{4\} = v_3\{6\} = v_3\{\mathrm{RP}\} = 0$), does not agree with the nonzero $\varepsilon_3\{4\}$ and $v_3\{4\}$ presented above. The Bessel-Gaussian function is therefore not a candidate of the underlying $p.d.f.$ of v_n and ε_n. On the other hand, because triangularity is expected to be solely created by initial geometry fluctuations, its distributions should be well reproduced by a single-parameter power-law function [43]. Indeed nice agreements between the fits of the power-law and the ε_3 distributions are observed for the presented centralities. When testing the two-parameter elliptic-power function, it turns out, as expected from the nice fit of the power-law function, that the parameter ε_0 (triangularity with respect to the reaction plane) is very close to 0. The nice descriptions of the ε_3 distributions by the power-law function and the elliptic-power function with parameter $\varepsilon_0 \sim 0$ confirm that the contributions of the reaction plane to ε_3 is very weak (or zero). This also agrees with our results of $v_3\{\mathrm{RP}\} = 0$, displayed in Fig. 4, and with the experimental measurements of ALICE [31]. Furthermore, we notice that the true $\sigma_{\varepsilon_3}/\varepsilon_3$ from the AMPT initial state shows a decreasing trend from central to peripheral collisions. This decreasing trend is captured by the elliptic-power function quite well, and clearly disagrees with the expectation of a Bessel-Gaussian type $p.d.f.$, which predicts a constant value of $\sqrt{4/\pi - 1}$ for the entire centrality range [10,38]. It is shown that the elliptic-power function gives a better description of the ε_2 and ε_3 distributions simultaneously, matches the

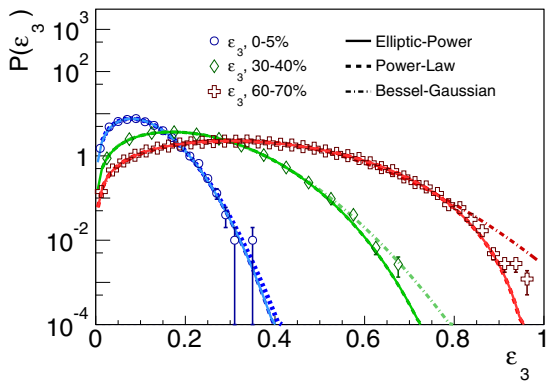

FIG. 6. ε_3 distributions in the AMPT initial state.

multiparticle cumulants observables and the correlations with respect to the reaction plane, and also matches the experimental measurements [31]. This shows that the elliptic-power distributions could be a promising candidate of the underlying $p.d.f.$ of v_n (and ε_n), which helps us to better understand the initial geometry and its event-by-event fluctuations.

In addition, it is important to understand whether there is a correlation between different order flow vectors, including both the flow planes (direction of the flow vector) and the harmonics (magnitude of the flow vector), and how this correlation between flow vectors modifies the underlying $p.d.f.$ One example of the correlation between different flow planes is the correlation of Ψ_2 and Ψ_3 measured using a five-particle cumulant:

$$v_3^2\{\Psi_2\} = \frac{\langle\cos(2\varphi_1 + 2\varphi_2 + 2\varphi_3 - 3\varphi_4 - 3\varphi_5)\rangle}{v_2^3}, \quad (23)$$

[32] (also denoted by $v_{23} \equiv v\{2,2,2,-3,-3\}$ in Ref. [44]). Figure 4(a) shows that $v_3^2\{\Psi_2\}$ from the AMPT model is consistent with zero, and because both v_2 and v_3 are nonzero, this result proves that there is no correlation between Ψ_2 and Ψ_3 in the AMPT calculations.

In addition to the correlations between the second- and third-order flow planes we can also study the correlations between the other order flow planes. These studies have recently gained a lot of attention in the field [20,42,44–46]. It was proposed to measure these correlations using the multiparticle mixed harmonic correlations [44]:

$$\begin{aligned}&\langle\cos(n_1\varphi_1 + \cdots + n_k\varphi_k)\rangle \\ &\quad = \langle v_{n_1}\ldots v_{n_k}\cos(n_1\Psi_{n_1} + \cdots + n_k\Psi_{n_k})\rangle. \end{aligned} \quad (24)$$

These new observables have been measured with $v_3^2\{\Psi_2\}$ in ALICE [31] and more detailed studies have been presented in a recent work [42]. Hydrodynamic calculations [20] predict that the correlation strength is sensitive to both the initial conditions and the details of the expansion of the system. AMPT simulations, which also provide information of the initial and final states, will help us to understand the role of these correlations in a cascade model.

Using Eq. (24), we can study the n^{th} and m^{th} order flow plane correlations in the final state. For example, the correlations between (Ψ_4, Ψ_2) and (Ψ_6, Ψ_3) can be evaluated via

$$\begin{aligned}\langle\cos(4\varphi_1 - 2\varphi_2 - 2\varphi_3)\rangle &= \langle v_4 v_2^2\cos(4\Psi_4 - 4\Psi_2)\rangle, \\ \langle\cos(6\varphi_1 - 3\varphi_2 - 3\varphi_3)\rangle &= \langle v_6 v_3^2\langle\cos(6\Psi_6 - 6\Psi_3)\rangle. \end{aligned} \quad (25)$$

As discussed in Ref. [32], these observables can be directly calculated in terms of a three-particle cumulant:

$$\begin{aligned}\mathrm{QC}\{3\}_{2n,-n,-n} &= \langle\cos[n(2\varphi_1 - \varphi_2 - \varphi_3)]\rangle \\ &= [Q_{2n}Q_n^*Q_n^* - 2\cdot|Q_n|^2 - |Q_{2n}|^2 + 2M]/ \\ &\quad [M(M-1)(M-2)]. \end{aligned} \quad (26)$$

For $n = 2$, we get $\mathrm{QC}\{3\}_{4,-2,-2}$ which is sensitive to the correlations between (Ψ_4, Ψ_2), and analogously for $n = 3$ which is sensitive to the correlations between (Ψ_6, Ψ_3).

In AMPT, we can also study correlations between the n^{th}- and m^{th}-order symmetry planes, in the initial state (Φ_n, Φ_m). In this model, we can calculate Φ_n assuming that the initial

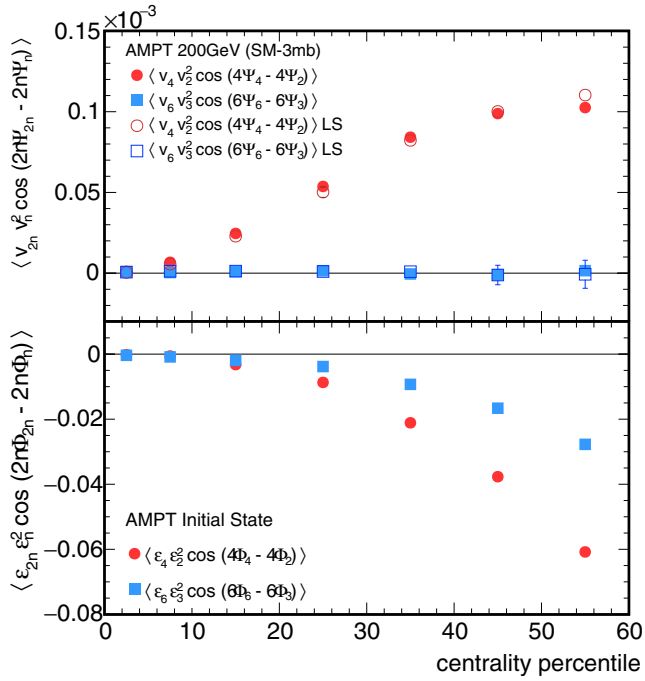

FIG. 7. Centrality dependence of the final state QC{3} (top) and the two-plane correlations in the initial state (bottom) in Au+Au collisions at 200 GeV by AMPT StringMelting.

spatial energy distribution is proportional to the initial spatial parton distribution. Thus, we have

$$\Phi_n = \frac{1}{n}\mathrm{ATan2}\left(\frac{\langle \sin(n\phi)\rangle}{\langle \cos(n\phi)\rangle} + \pi\right), \tag{27}$$

where ϕ is the azimuthal angle of the initial partons.

For the (Φ_n, Φ_m) correlation, we can use, similar to Eq. (25),

$$\langle \cos(4\phi_1 - 2\phi_2 - 2\phi_3)\rangle = \left\langle \varepsilon_4\varepsilon_2^2 \cos(4\Phi_4 - 4\Phi_2)\right\rangle,$$
$$\langle \cos(6\phi_1 - 3\phi_2 - 3\phi_3)\rangle = \left\langle \varepsilon_6\varepsilon_3^2 \cos(6\Phi_6 - 6\Phi_3)\right\rangle. \tag{28}$$

If the initial state symmetry plane Φ_n coincides with the flow plane Ψ_n, the initial (Φ_n, Φ_m) correlation and the final (Ψ_n, Ψ_m) correlation should show a similar centrality dependence, and at least should have the same sign.

We see in Fig. 7 (top) that the (Ψ_4, Ψ_2) correlation has a positive sign, which increases as the centrality increases. In contrast, the (Φ_4, Φ_2) correlation is negative and decreases with increasing centrality, plotted in Fig. 4 (bottom). The negative initial (Φ_4, Φ_2) correlation and positive final (Ψ_4, Ψ_2) correlation observed in the AMPT model are in qualitative agreement with viscous hydrodynamic calculations [20]. There is a clear sign change of the fourth-order and second-order plane correlation during the collision system evolution, both in the transport model and in the hydrodynamic calculations [20]. On the other hand, the sixth-order and third-order plane correlation has a negative value in the initial (Φ_6, Φ_3) correlations while it is consistent with 0 within uncertainty in the final state (Ψ_6, Ψ_3) correlations. In addition, we can see in Fig. 4 (top) that there is no clear difference of the QC{3} from all charged particles (solid symbols) and the like-sign (LS) particles (open symbols), which indicates that nonflow contributions to the above observables are small and the sign change of the plane correlations cannot be explained by the possible nonflow contributions.

Considering that the initial anisotropy ε_n and the final anisotropic flow v_n are both positive, the above results can only be explained if the sign of the genuine correlation, the cosine component, changes during the evolution of the produced system. In fact, hydrodynamic calculations suggest that the final n^{th}-order flow plane Ψ_n might be not only driven by Φ_n, but might also have contributions from other symmetry plane(s). The fourth-order harmonic v_4 and its associated flow plane Ψ_4 are determined by a linear and a quadratic response [47],

$$v_4\, e^{-i\,4\,\Psi_4} = w_4\, e^{-i\,4\,\Phi_4} + w_{4\,(22)}\, e^{-i\,4\,\Phi_2}, \tag{29}$$

where w_4 describes the linear response, and $w_{4\,(22)}$ quantifies the nonlinear response. This nonlinear response in hydrodynamic calculations couples v_4 to $(v_2)^2$ and also couples v_6 to v_3^2 [47], and clearly both Φ_2 and Φ_4 contribute to Ψ_4. Therefore, these results show that the initial symmetry plane Φ_n and the flow plane Ψ_n do not coincide in the AMPT model. Similar results were also observed in the previous transport model calculations using the UrQMD model [48], and confirmed by hydrodynamic calculations [49]. Thus, the assumption $\Phi_n = \Psi_n$ used in the so-called true flow calculations (or symmetry plane flow) $v_n\{\Phi_n\}$ [16,50,51] is not valid. In addition, we notice that a new method, named the scalar product method [45], is proposed to measure the flow plane correlations without contributions of anisotropic flow. However, it is important to emphasize that this method is based on the assumption that $\langle v_n^2 v_{2n}\rangle = \langle v_n^2\rangle\sqrt{\langle v_{2n}^2\rangle}$. In fact, the recent "standard candle" calculations $SC(m,n,-m,-n)_v$ [52,53] have shown that there are strong (anti-)correlations between event-by-event fluctuations of v_n and v_m, therefore the equality $\langle v_n^2 v_{2n}\rangle = \langle v_n^2\rangle\sqrt{\langle v_{2n}^2\rangle}$ assumed in the scalar product method does not hold. Thus, in this paper, we discuss the symmetry plane correlations using only the mixed harmonic correlations.

Not only the correlations between symmetry planes but also the correlations between different flow harmonics can be investigated via the multiparticle correlation technique. The observable $SC(m,n,-m,-n)_v$ was proposed as a unique tool to probe the correlations between different orders of flow harmonics and by design independent of the symmetry planes [52].

In Fig. 8 (top) we see a clear nonzero value for both $SC(4,2,-4,-2)_v$ (red markers) and $SC(3,2,-3,-2)_v$ (blue markers) in the final state. The positive results of $SC(4,2,-4,-2)_v$ and negative results of $SC(3,2,-3,-2)_v$ are observed for the presented centrality classes. These (anti-)correlations are more pronounced in peripheral collisions. It indicates that finding v_2 larger than $\overline{v}_2$ in an event enhances the probability of finding v_4 larger than $\overline{v}_4$ and, in addition, the probability of finding v_3 smaller than $\overline{v}_3$ in that event, as was shown in a previous study [52]. Also we investigate the correlations of the n^{th}- and m^{th}-order harmonics in the initial state, calculating

$$SC(m,n,-m,-n)_\varepsilon = \left\langle \varepsilon_m^2\, \varepsilon_n^2\right\rangle - \left\langle \varepsilon_m^2\right\rangle\left\langle \varepsilon_n^2\right\rangle. \tag{30}$$

The result is presented in Fig. 8 (bottom). We see a positive and increasing trend for $SC(4,2,-4,-2)_\varepsilon$ while a negative and

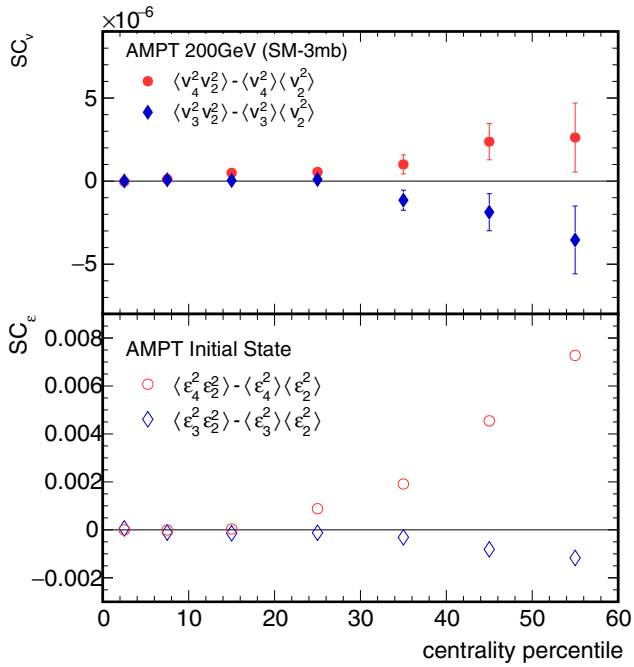

FIG. 8. Centrality dependence of correlations between the n^{th}- and m^{th}-order harmonics in the final state (top) and initial state (bottom) in Au+Au collisions at 200 GeV by AMPT StringMelting.

decreasing trend of $SC(3,2,-3,-2)_\varepsilon$ is observed. They capture the rough trend of $SC(4,2,-4,-2)_v$ and $SC(3,2,-3,-2)_v$ in the final state but cannot quantitatively describe the centrality dependence. This suggests indeed a correlation between the initial state $SC(m,n,-m,-n)_\varepsilon$ and final state $SC(m,n,-m,-n)_v$, but this might not be the only contribution to the final state. In addition, the system evolution might also modify the strength of $SC(m,n,-m,-n)_v$. In a previous study [52], three configurations of the AMPT model [(a) 3 mb, (b) 10 mb, and (c) 10 mb no rescattering] have been investigated to better understand the $SC(m,n,-m,-n)_v$ calculations. In general, the configuration of (a) 3 mb generates weaker partonic interactions during the system evolution compared to (b) 10 mb. And the hadronic interactions are turned off for (c) 10 mb no rescattering. The comparisons between these three configurations shows that the value of $SC(m,n,-m,-n)_v$ depends on both the partonic and the hadronic interactions. These results suggest that the sign of $SC(m,n,-m,-n)_v$ is determined by the initial state $SC(m,n,-m,-n)_\varepsilon$ and the magnitude is modified by the multiple interactions during the system evolution.

As we discussed above, the elliptic-power function gives a better description of the $p.d.f.$ of each single harmonic. However, it is an open question at the moment how the joint underlying $p.d.f.$ including different order symmetry planes and harmonics is described and, additionally, if these correlations between different order symmetry planes and harmonics modify the single harmonics $p.d.f.$ The investigations presented here begin to answer these open questions. Nevertheless, many more measurements between different order symmetry planes and harmonics are necessary to reasonably constrain a joint $p.d.f.$, and ultimately lead to new insights into the nature of the fluctuation of the created matter in heavy ion collisions.

V. SUMMARY

In this paper we presented the calculations of the initial and final state anisotropies in Au+Au collisions at $\sqrt{s_{\text{NN}}} =$ 200 GeV using AMPT simulations. It is found that the elliptic-power function is the only $p.d.f.$ so far which describes the event-by-event distributions of the eccentricity as well as the triangularity, the anisotropic flow from multiparticle cumulants, and the relative flow fluctuations very well. In addition, the correlations between different order symmetry planes and harmonics have been investigated. A different centrality dependence of these correlations in the initial and final state was observed within the same framework of a transport model. This result indicates that both the fluctuations in the initial geometry and the dynamical evolution of the medium in the final state plays an important role. It is currently still unclear how well the underlying joint $p.d.f.$ matches the experimental data as these predictions still have to be tested at RHIC and at the LHC. The study presented in this paper should help us better understand the fluctuations of created matter in heavy ion experiments.

ACKNOWLEDGMENTS

The authors thank A. Bilandžić, R. Bertens, and K. Gulbrandsen for the comments on the manuscript, and P. Christakoglou, A. Tang, S. Voloshin, and F. Q. Wang for fruitful discussion. Part of this work is inspired by the discussion with J. Y. Ollitrault. The authors are supported by the Danish Council for Independent Research, Natural Sciences, and the Danish National Research Foundation (Danmarks Grundforskningsfond), MOST of China under 973 Grant No. 2015CB856901, the National Natural Science Foundation of China (NSFC) under Grants No. 11135011, No. 11228513, and No. 11221504, FOM, and NWO of the Netherlands.

[1] S. Voloshin and Y. Zhang, Z. Phys. C **70**, 665 (1996).
[2] C. Alt *et al.* (NA49 Collaboration), Phys. Rev. C **68**, 034903 (2003).
[3] K. H. Ackermann *et al.* (STAR Collaboration), Phys. Rev. Lett. **86**, 402 (2001); C. Adler *et al.* (STAR Collaboration), *ibid.* **87**, 182301 (2001); Phys. Rev. C **66**, 034904 (2002).
[4] K. Adcox *et al.* (PHENIX Collaboration), Phys. Rev. Lett. **89**, 212301 (2002); S. S. Adler *et al.* (PHENIX Collaboration), *ibid.* **91**, 182301 (2003).
[5] B. B. Back *et al.* (PHOBOS Collaboration), Phys. Rev. Lett. **89**, 222301 (2002).
[6] K. Aamodt *et al.* (ALICE Collaboration), Phys. Rev. Lett. **105**, 252302 (2010).

[7] G. Aad *et al.* (ATLAS Collaboration), Phys. Lett. B **707**, 330 (2012).
[8] S. Chatrchyan *et al.* (CMS Collaboration), Eur. Phys. J. C **72**, 2012 (2012).
[9] J.-Y. Ollitrault, Phys. Rev. D **46**, 229 (1992).
[10] S. A. Voloshin, A. M. Poskanzer, and R. Snellings, in *Landolt-Boernstein, Relativistic Heavy Ion Physics*, Vol. 1/23 (Springer-Verlag, Berlin, 2010), pp. 5–54.
[11] R. Snellings, New J. Phys. **13**, 055008 (2011).
[12] V. P. Konchakovski, V. D. Toneev, W. Cassing, E. L. Bratkovskaya, S. A. Voloshin, and V. Voronyuk, J. Phys. Conf. Ser. **389**, 012015 (2012).
[13] M. Luzum and H. Petersen, J. Phys. G **41**, 063102 (2014).
[14] R. Snellings, J. Phys. G **41**, 124007 (2014).
[15] J. Jia, J. Phys. G **41**, 124003 (2014).
[16] B. Alver and G. Roland, Phys. Rev. C **81**, 054905 (2010); **82**, 039903(E) (2010).
[17] B. H. Alver, C. Gombeaud, M. Luzum, and J.-Y. Ollitrault, Phys. Rev. C **82**, 034913 (2010).
[18] W. T. Deng, Z. Xu, and C. Greiner, Phys. Lett. B **711**, 301 (2012).
[19] H. Niemi, K. J. Eskola, and R. Paatelainen, Phys. Rev. C **93**, 024907 (2016).
[20] Z. Qiu and U. Heinz, Phys. Lett. B **717**, 261 (2012).
[21] Z.-W. Lin, C. M. Ko, B.-A. Li, B. Zhang, and S. Pal, Phys. Rev. C **72**, 064901 (2005).
[22] X.-N. Wang and M. Gyulassy, Phys. Rev. Lett. **86**, 3496 (2001).
[23] B. Zhang, Comput. Phys. Commun. **109**, 193 (1998).
[24] L.-W. Chen and C. M. Ko, Phys. Lett. B **634**, 205 (2006).
[25] B.-A. Li and C. M. Ko, Phys. Rev. C **52**, 2037 (1995).
[26] J. Xu and C. M. Ko, Phys. Rev. C **84**, 014903 (2011).
[27] B. Abelev *et al.* (ALICE Collaboration), Phys. Lett. B **723**, 267 (2013).
[28] N. Borghini, P. M. Dinh, and J.-Y. Ollitrault, Phys. Rev. C **64**, 054901 (2001).
[29] A. Bilandžić, R. Snellings, and S. Voloshin, Phys. Rev. C **83**, 044913 (2011).
[30] G. Agakishiev *et al.* (STAR Collaboration), Phys. Rev. C **86**, 014904 (2012).
[31] K. Aamodt *et al.* (ALICE Collaboration), Phys. Rev. Lett. **107**, 032301 (2011).
[32] A. Bilandžić, Ph.D thesis, Nikhef and Utrecht University, The Netherlands, 2012.
[33] Y. Zhou (ALICE Collaboration), Nucl. Phys. A **931**, 949 (2014).
[34] M. Miller and R. Snellings, arXiv:nucl-ex/0312008.
[35] X. Zhu, M. Bleicher, and H. Stoecker, Phys. Rev. C **72**, 064911 (2005).
[36] H. Niemi, G. S. Denicol, H. Holopainen, and P. Huovinen, Phys. Rev. C **87**, 054901 (2013).
[37] S. A. Voloshin, A. M. Poskanzer, A. Tang, and G. Wang, Phys. Lett. B **659**, 537 (2008).
[38] W. Broniowski, P. Bozek, and M. Rybczynski, Phys. Rev. C **76**, 054905 (2007).
[39] L. Yan, J. Y. Ollitrault, and A. M. Poskanzer, Phys. Rev. C **90**, 024903 (2014).
[40] L. Yan and J. Y. Ollitrault, Phys. Rev. Lett. **112**, 082301 (2014).
[41] Y. Zhou (ALICE Collaboration), Acta Phys. Polon. Supp. **5**, 407 (2012).
[42] A. Bilandžić (ALICE Collaboration), Nucl. Phys. A **904-905**, 515c (2013).
[43] L. Yan, J. Y. Ollitrault, and A. M. Poskanzer, Phys. Lett. B **742**, 290 (2015).
[44] R. S. Bhalerao, M. Luzum, and J.-Y. Ollitrault, Phys. Rev. C **84**, 034910 (2011).
[45] R. S. Bhalerao, J. Y. Ollitrault, and S. Pal, Phys. Rev. C **88**, 024909 (2013).
[46] J. Jia (ATLAS Collaboration), Nucl. Phys. A **910-911**, 276 (2013).
[47] D. Teaney and L. Yan, Phys. Rev. C **86**, 044908 (2012).
[48] H. Petersen, G. Y. Qin, S. A. Bass, and B. Muller, Phys. Rev. C **82**, 041901 (2010).
[49] Z. Qiu and U. W. Heinz, Phys. Rev. C **84**, 024911 (2011).
[50] G.-L. Ma and X.-N. Wang, Phys. Rev. Lett. **106**, 162301 (2011).
[51] L. Ma, G. L. Ma, and Y. G. Ma, Phys. Rev. C **89**, 044907 (2014).
[52] A. Bilandzic, C. H. Christensen, K. Gulbrandsen, A. Hansen, and Y. Zhou, Phys. Rev. C **89**, 064904 (2014).
[53] R. S. Bhalerao, J. Y. Ollitrault, and S. Pal, Phys. Lett. B **742**, 94 (2015).